



CHALMERS

Chalmers Publication Library

Calibration, Validation and Uncertainty Quantification of Nominally Identical Car Subframes

This document has been downloaded from Chalmers Publication Library (CPL). It is the author's version of a work that was accepted for publication in:

Model Validation and Uncertainty Quantification, Volume 3, Proceedings of the 34th IMAC, A Conference and Exposition on Structural Dynamics 2016 (ISSN: 2191-5644)

Citation for the published paper:

Gibanica, M. ; Abrahamsson, T. ; Olsson, M. (2016) "Calibration, Validation and Uncertainty Quantification of Nominally Identical Car Subframes". Model Validation and Uncertainty Quantification, Volume 3, Proceedings of the 34th IMAC, A Conference and Exposition on Structural Dynamics 2016, vol. 3 pp. 315-326.

http://dx.doi.org/10.1007/978-3-319-29754-5_31

Downloaded from: <http://publications.lib.chalmers.se/publication/239001>

Notice: Changes introduced as a result of publishing processes such as copy-editing and formatting may not be reflected in this document. For a definitive version of this work, please refer to the published source. Please note that access to the published version might require a subscription.

Chalmers Publication Library (CPL) offers the possibility of retrieving research publications produced at Chalmers University of Technology. It covers all types of publications: articles, dissertations, licentiate theses, masters theses, conference papers, reports etc. Since 2006 it is the official tool for Chalmers official publication statistics. To ensure that Chalmers research results are disseminated as widely as possible, an Open Access Policy has been adopted. The CPL service is administrated and maintained by Chalmers Library.

Calibration, validation and uncertainty quantification of nominally identical car subframes

Mladen Gibanica^{1,2}, Thomas J. S. Abrahamsson¹, Magnus Olsson²

¹Applied Mechanics, Chalmers University of Technology, Hörsalsvägen 7A, S-41296 Göteborg, Sweden

²Volvo Car Corporation, S-40531 Göteborg, Sweden

e-mail: mladen.gibanica@chalmers.se

ABSTRACT

In this paper a finite element model, with over half a million degrees-of-freedom, of a car front subframe has been calibrated and validated against experimental MIMO data of several nominally identical components. The spread between the individual components has been investigated and is reported. Sensor positioning was performed with an extended effective independence method, using system gramians to reject sensors with redundant information. The Fisher information matrix was used in the identification of the most significant model calibration parameters. Validation of the calibrated model was performed to evaluate the difference between the nominal and calibrated model, and bootstrapping used to investigate the validity of the calibrated parameters. The parameter identification, calibration, validation and bootstrapping have been performed using the open-source MATLAB tool FEMcali.

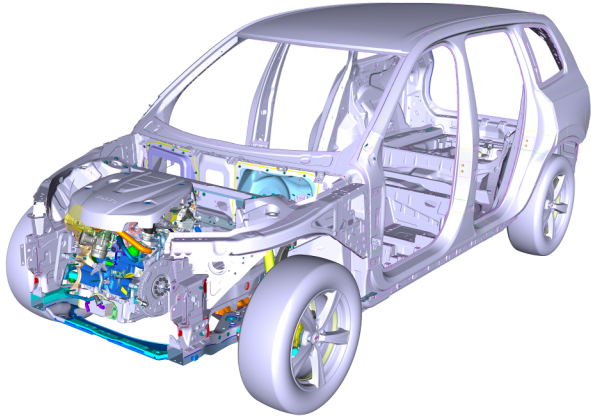
Keywords: model updating, uncertainty quantification, parameter identification, bootstrapping, FEMcali.

1 Introduction

Finite element (FE) modelling is commonly used in many industries today, including the automotive industry, for research and development purposes. It allows for very quick and cost efficient design alterations of complicated models, compared to prototype models, which is crucial in advanced industries. However, there are drawbacks in terms of the confidence engineers can have in their FE models. To address this issue, verification is usually performed to verify that the FE solver is free from errors and the mesh is sufficiently fine such that the underlying mathematical model is properly solved. The FE model can then be compared to an experimental model, usually acquired through experimental modal analysis (EMA) [1], in a procedure denoted model validation. If the FE model does not predict the responses acquired from the experimental model, to within some given tolerances, it is possible to update the model. This step is called calibration, or model updating, which seeks to minimise some deviation metric between the two models [2].

It is well known that mass produced components exhibit some amount of spread in dynamic and static properties between individuals in a population. The spread can originate from multiple sources such as material spread and geometry spread, to name a few. In the automotive industry it is common to have thousands of nominally identical components, and even whole cars, that are supposed to be represented by one FE model. Validating and calibrating against one of these components will not necessarily produce a model that better captures the characteristics of another, nominally identical, component. Therefore, it is of interest to quantify the spread between the individuals and to calibrate and validate towards some sample set from the whole population.

In a recently initiated project at Volvo Car Corporation, the goal is to better understand the uncertainties in components and their propagation through other components. This paper presents the first part of the project where three nominally identical front subframes of a Volvo XC90 (2015) have been studied, shown in Figure 1. The component properties are important since it provides support for the engine and connects the suspension link arms to the car body. This means that vibrations are transferred through the component and further to the driver and passengers. It is also an important part from a safety perspective as a crash



(a) Parts of an XC90



(b) Front subframe location in the car

Figure 1 The front subframe is an important part from a vibration perspective as it connects the suspension link arms and engine to the car body

box is attached to it. Therefore it is of interest to investigate this component thoroughly.

In this paper the calibration was performed with the open-source tool FEMcali as described in reference [3]. The method works by creating a parametrised surrogate model of the FE model and it then seeks to minimise a deviation metric between the created surrogate and experimental model's frequency response functions (FRFs) using normalised damping in both models. Previous work using this method has been performed on various industrial components with good results [4–7]. Pretest planning has been performed with the expansion method of effective independence (Efi) [8] with an added gramian rejection step, described further in [9]. The three components were tested in a vibration-test with an improved frequency strategy [10] for subspace state-space system identification [11]. The FE model consists of a 556,758 degrees-of-freedom mesh and has been calibrated against all three components. Bootstrapping has been used in order to quantify the uncertainty in the chosen calibration parameters.

The paper is organised as follows. In Section 2 the theoretical part of the calibration procedure is presented briefly and in Section 3 the vibration testing is explained and the finite element model presented. In Section 4 the findings from calibration, validation and bootstrapping are shown. Section 5 concludes the paper.

2 Theory

A brief overview of the theory presented in [3], where the calibration and validation methods used in this paper are presented, is recited here.

2.1 Mechanical systems theory

The equations of motion for a mechanically vibrating system can be written as

$$\mathbf{M}\ddot{\mathbf{q}} + \mathbf{V}\dot{\mathbf{q}} + \mathbf{K}\mathbf{q} = \mathbf{f}(t) \quad (1)$$

where \mathbf{M} , \mathbf{V} and $\mathbf{K} \in \mathbb{R}^{m \times m}$ represent the mass, damping and stiffness matrices, respectively. The general displacement vector is denoted by \mathbf{q} and the external force vector by $\mathbf{f}(t)$. The dot notation is used for time differentiation. The full load vector can be mapped to the input vector $\mathbf{u} \in \mathbb{R}^{n_u}$ with the Boolean transformation matrix \mathbf{U} as $\mathbf{f} = \mathbf{U}\mathbf{u}$. A parametrisation of the mass and stiffness matrices, \mathbf{M} and \mathbf{K} , can be made where the physical parameters are placed in a vector $\mathbf{P} \in \mathbb{R}^{n_p}$. The parametrised mass and stiffness matrices can then be expressed as $\mathbf{M} = \mathbf{M}(\mathbf{P})$ and $\mathbf{K} = \mathbf{K}(\mathbf{P})$. Minimiser methods usually work better with scaled unknowns, and thus the parameter vector \mathbf{P} can be related to a normalised parameter vector \mathbf{p} and some fixed non-zero nominal parameter setting \mathbf{P}_0 so that $\mathbf{P} = \mathbf{P}_0(1 + \mathbf{p})$ holds [3].

The system on second order form in Equation (1) can be transformed to first order form by forming the state vector $\mathbf{x} = [\mathbf{q}^T, \dot{\mathbf{q}}^T]^T$ and using the dummy equation $\mathbf{I}\ddot{\mathbf{q}} - \mathbf{I}\dot{\mathbf{q}} = 0$ which gives

$$\begin{cases} \dot{\mathbf{x}} = \mathbf{Ax} + \mathbf{Bu} \\ \mathbf{y} = \mathbf{Cx} + \mathbf{Du} \end{cases} \quad (2)$$

with $\mathbf{A} \in \mathbb{R}^{n \times n}$ representing the system matrix, $\mathbf{B} \in \mathbb{R}^{n \times n_u}$ representing the input matrix, $\mathbf{C} \in \mathbb{R}^{n_y \times n}$ representing the output matrix, $\mathbf{D} \in \mathbb{R}^{n_y \times n_u}$ representing the force throughput matrix and \mathbf{y} representing the system outputs. The relationship between n and m is $n = 2m$. The system matrices can be shown to be

$$\mathbf{A} = \begin{bmatrix} \mathbf{0} & \mathbf{I} \\ -\mathbf{M}^{-1}\mathbf{K} & -\mathbf{M}^{-1}\mathbf{V} \end{bmatrix} \quad \mathbf{B} = \begin{bmatrix} \mathbf{0} \\ \mathbf{M}^{-1}\mathbf{U} \end{bmatrix} \quad (3)$$

where \mathbf{C} and \mathbf{D} are formed appropriately so that linear combinations of the system states \mathbf{x} and inputs \mathbf{u} form the system outputs \mathbf{y} .

2.2 Calibration, validation and bootstrapping

A deviation metric that is smooth and does not discriminate against low structural responses is used in a gradient based minimiser during the calibration procedure. The deviation metric used, as a metric for both calibration and validation is

$$\delta = \frac{\boldsymbol{\varepsilon}^T \boldsymbol{\varepsilon}}{N} \quad \text{with} \quad \boldsymbol{\varepsilon}(\mathbf{p}) = \log_{10} \text{vect}(\mathbf{H}^A(\mathbf{p})) - \log_{10} \text{vect}(\mathbf{H}^X) \quad (4)$$

where the transfer function matrix \mathbf{H}^X stand for the experimental model representation and $\mathbf{H}^A(\mathbf{p})$ stand for the FE model representation, at parameter \mathbf{p} . Here N stands for the total number of data points in the FRF matrix, as explained below. The transfer function matrix can be formed from the system in Equation (2), at frequency ω_i , as

$$\mathbf{H}(\omega_i) = \mathbf{C}(j\omega_i \mathbf{I} - \mathbf{A})^{-1} \mathbf{B} + \mathbf{D} \quad (5)$$

where j given by $j^2 = -1$ is the imaginary number and \mathbf{I} the identity matrix of appropriate dimension. Here $\text{vect}(\cdot)$ stands for the vectorisation operation in which a matrix is transformed into a vector by stacking the columns of the matrix. Therefore the transfer function matrix $\mathbf{H} \in \mathbb{C}^{n_y \times n_u}$ at each frequency step with n_f frequency steps in total is transformed into an $n_y n_u n_f \times 1$ column vector.

The deviation metric must be evaluated at the same frequencies for the FE and experimental model. Therefore a system identification procedure is introduced in order to obtain a state-space system on the form shown in Equation (2) where the identified system can be evaluated at any frequency. This step is also necessary for damping equalisation mentioned below, and in addition removes the noise found in the measured data. The calibration metric is comparing the FE model with the identified model and it is therefore crucial that the identified model is very well estimated. In this paper the N4SID, linear subspace state-space system identification, method is used [11].

In [3] the authors advise in selecting the frequencies based on the half-band width, $\Delta\omega_i$, of the eigenmodes. The half-band width for a damped structural resonance at a certain frequency ω_i can be expressed as $\Delta\omega_i = 2\xi_i \omega_i$ where ξ_i is the i :th relative modal damping. This is used in the calibration procedure, but in the EMA frequency lines were selected based on a more recent paper by Vakilzadeh et al. [10] in which the authors advise in another selection strategy for improving the estimated state-space system with the N4SID method [11].

The obtained data from an EMA is split into two sets, one for a classical leave out validation \mathbf{H}_v^X and the other for calibration \mathbf{H}_c^X . While classical leave out validation is used to verify that the calibrated model is in fact improved on, by letting it make predictions on previously unseen data, bootstrapping is commonly used in many fields for quantifying the uncertainty in model parameters [12]. It works by resampling the calibration data set $\mathbf{q} = \text{vect}(\mathbf{H}_c^X) = \{\mathbf{q}_1 \dots \mathbf{q}_{n^X}\}$, with $n^X = n_y^X n_u^X n_f^X$ and superscript X representing the calibration data set, such that k random draws are taken where each draw is the same length as \mathbf{q} and can contain overlapping data. Statistical properties can then be evaluated from these k models and used to quantify the uncertainty in the calibration parameters.

2.3 Damping equalisation

Since damping is very hard to model and is crucial in FRF based model calibration it is often assigned as a simple representation in the FE model. Commonly the damping is measured in an experimental modal analysis experiment and the measured value is assigned to the FE model. The issue then is that damping usually varies between modes which make it very hard to map an experimental model's damping to a complex FE model with high mode density. Therefore, damping equalisation was proposed

in [3]. The same level of damping is enforced for all modes in both the FE model and identified model from the experimental model, rendering mode pairing unnecessary.

The state-space system in Equation (2) can be brought to diagonal form by a similarity transformation, here being the eigenvector matrix \mathbf{X} of the eigenvalue problem $\mathbf{AX} = \mathbf{X}\Lambda$ where Λ is the diagonal eigenvalue matrix. With coordinate transformation $\mathbf{x} = \mathbf{Xz}$ the diagonal system becomes

$$\begin{cases} \dot{\mathbf{z}} = \mathbf{X}^{-1}\mathbf{AXz} + \mathbf{X}^{-1}\mathbf{Bu} \\ \mathbf{y} = \mathbf{CXz} + \mathbf{Du} \end{cases} \quad (6)$$

where $\mathbf{X}^{-1}\mathbf{AX} = \tilde{\mathbf{A}} = \text{diag}(\lambda_i)$ and λ_i is the i :th complex valued system pole. For small damping the relative damping ξ_i is

$$\xi_i = -\frac{\mathbb{R}(\lambda_i)}{|\mathbb{C}(\lambda_i)|} \quad (7)$$

where $|\cdot|$ represent the absolute value and $\mathbb{R}(\cdot)$ and $\mathbb{C}(\cdot)$ represent the real and complex part of an imaginary number, respectively. In the damping equalisation step all modal damping are set to a fixed value $\xi_i = \xi_0 \forall i$. Thus a new system is obtained

$$\begin{cases} \dot{\mathbf{z}} = \tilde{\mathbf{A}}\mathbf{z} + \mathbf{X}^{-1}\mathbf{Bu} \\ \mathbf{y} = \mathbf{CXz} + \mathbf{Du} \end{cases} \quad (8)$$

with $\tilde{\mathbf{A}} = \text{diag}(\tilde{\lambda}_i)$ and

$$\tilde{\lambda}_i = \mathbb{C}(\lambda_i)(-\xi_0 + i) \quad \forall \mathbb{C}(\lambda_i) > 0, \quad \tilde{\lambda}_i = \mathbb{C}(\lambda_i)(\xi_0 + i) \quad \forall \mathbb{C}(\lambda_i) < 0. \quad (9)$$

The FE model's modal viscous damping can then be formed as [13]

$$\mathbf{V} = \mathbf{MXdiag}(m_i^{-1})\text{diag}(2\xi_0 m_i \omega_i)\text{diag}(m_i^{-1})\mathbf{X}^T \mathbf{M} \quad (10)$$

where ω_i are the eigenfrequencies, m_i the modal masses and \mathbf{X} the eigenvector matrix from the undamped eigenvalue problem of the system in Equation (1), $\mathbf{KX} = \mathbf{MXdiag}(\omega_i^2)$.

2.4 Model reduction

In industry, very large FE models are commonly used that may consist of more than millions degrees-of-freedom. It is therefore not feasible to perform model calibration on full scale models, but rather on reduced or surrogate models. The eigenvector matrix at the nominal parameter setting \mathbf{T} is used as a reduction basis and is kept constant during the calibration procedure, which is formed from the undamped eigenvalue problem of the system in Equation (1).

$$\mathbf{K}(\mathbf{p}_0)\mathbf{T} = \mathbf{M}(\mathbf{p}_0)\mathbf{T}\Omega, \quad \Omega = \text{diag}(\omega_i^2) \quad \forall \omega = [\omega_{low}, \omega_{high}] \quad (11)$$

Here $[\omega_{low}, \omega_{high}]$ represent the frequency range of interest. It is now possible to form the reduced mass and stiffness matrices at any parameter setting \mathbf{p}

$$\bar{\mathbf{M}}(\mathbf{p}) = \mathbf{T}^T \mathbf{M}(\mathbf{p}) \mathbf{T}, \quad \bar{\mathbf{K}}(\mathbf{p}) = \mathbf{T}^T \mathbf{K}(\mathbf{p}) \mathbf{T} \quad (12)$$

with the reduced mass and stiffness matrices at the nominal parameter setting \mathbf{p}_0 being represented by $\bar{\mathbf{M}}_0$ and $\bar{\mathbf{K}}_0$. Gradients of the reduced mass and stiffness matrices are

$$\bar{\mathbf{M}}_j = \mathbf{T}^T \left(\frac{d\mathbf{M}}{dp_j} \Big|_{p=p_0} \right) \mathbf{T}, \quad \bar{\mathbf{K}}_j = \mathbf{T}^T \left(\frac{d\mathbf{K}}{dp_j} \Big|_{p=p_0} \right) \mathbf{T} \quad (13)$$

for the i :th calibration parameters. By taking the first order expansions of the Taylor series of the reduced mass $\bar{\mathbf{M}}$ and stiffness $\bar{\mathbf{K}}$ matrices about \mathbf{p}_0 it is possible to form a surrogate model that is linear in the parameters.

$$\tilde{\mathbf{M}}(\mathbf{p}) = \bar{\mathbf{M}}_0 + \sum_{j=1}^{n_p} (p_j - p_{j,0}) \bar{\mathbf{M}}_j, \quad \tilde{\mathbf{K}}(\mathbf{p}) = \bar{\mathbf{K}}_0 + \sum_{j=1}^{n_p} (p_j - p_{j,0}) \bar{\mathbf{K}}_j \quad (14)$$

The new state-space matrix quadruple $\{\tilde{\mathbf{A}}, \tilde{\mathbf{B}}, \tilde{\mathbf{C}}, \tilde{\mathbf{D}}\}$ can be formed with a state transformation $\mathbf{x} = \mathbf{T}\xi$ and with a viscous damping matrix $\tilde{\mathbf{V}}$ formed as in Equation (10).

$$\tilde{\mathbf{A}} = \begin{bmatrix} \mathbf{0} & \mathbf{I} \\ -\tilde{\mathbf{M}}^{-1}\tilde{\mathbf{K}} & -\tilde{\mathbf{M}}^{-1}\tilde{\mathbf{V}} \end{bmatrix} \quad \tilde{\mathbf{B}} = \begin{bmatrix} \mathbf{0} \\ \tilde{\mathbf{M}}^{-1}\mathbf{T}^T\mathbf{U} \end{bmatrix} \quad \tilde{\mathbf{C}} = \begin{bmatrix} \mathbf{T} & \mathbf{0} \\ \mathbf{0} & \mathbf{T} \end{bmatrix} \quad \tilde{\mathbf{D}} = \mathbf{D} \quad (15)$$

Its frequency response functions can then be evaluated using Equation (5).

3 Experimental and FE model preparation

In this section the experimental modal analysis is explained in detail followed by an explanation of the FE model and the calibration parameter selection.

3.1 Experimental modal analysis

The structure considered is a front subframe of a Volvo XC90 (2015). Three individual subframes were used in this paper, which focuses on the spread in dynamic properties of these. The subframes were also weighted. A steel frame support structure was mounted in which the components were hung, at the exhaust hangers, in long thin high-strength lines, see Figure 2a, attached to steel springs on the supporting structure for a low bounce rigid body mode. Thus, the subframes were efficiently isolated from its surrounding and the rigid body modes were kept low, with eigenfrequencies below 5 Hz.

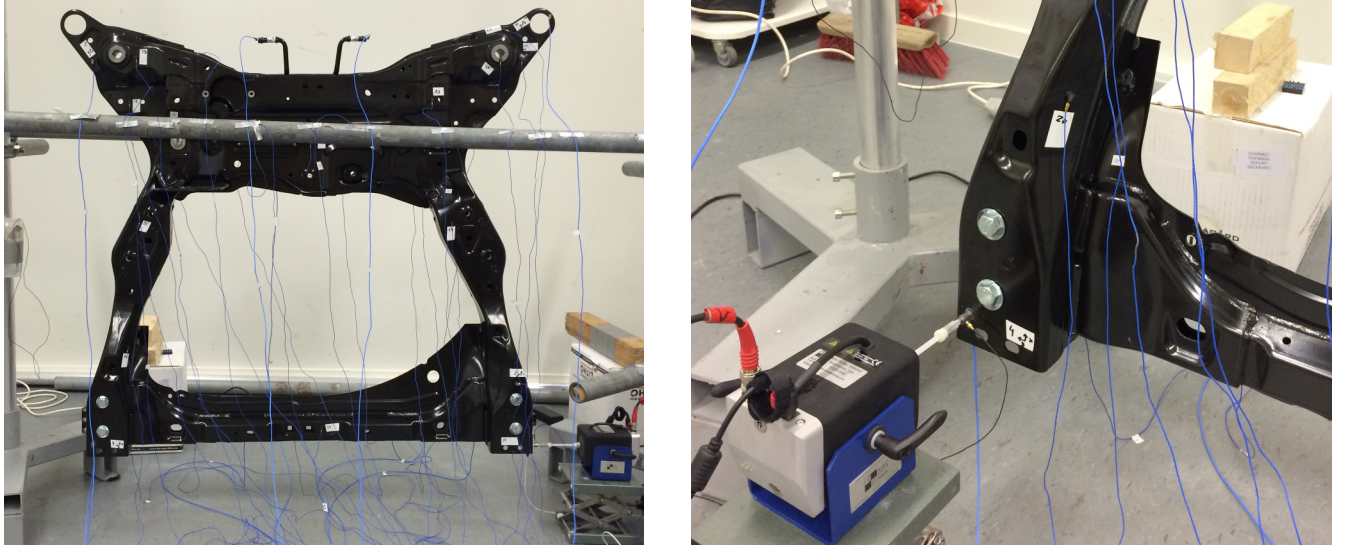
Sensor positions were selected by the modified set expansion Efl [8] algorithm with added gramian rejection for nodes containing similar information [9]. The candidate set consisted of 170 possible locations, or 510 degrees-of-freedom. The 10 triaxial accelerometers were placed first, with a rejection threshold of $T_s = 0.05$, see [9]. Two accelerometers were initially positioned at the exhaust hangers seen at the top middle in Figure 2a. These positions were selected as a few local modes excited these parts and it was of interest to find their vibration pattern. Then 15 uniaxial accelerometers were positioned, with a rejection threshold of $T_s = 0.01$, from an initial set of the 10 triaxial accelerometers previously positioned. The last 12 uniaxial accelerometers were placed for visualisation purposes. In the end only 31 accelerometers, shown in Figure 3, were used for calibration and validation. Two input locations were used, one seen in Figure 2a and the other seen in Figure 2b. The second input was added to capture an edge wise mode, mode 6 in Figure 5g. The shaker used was a Modal Shop type K2007E01 with a plastic stinger. This shaker was compared to another shaker, Ling Dynamic Systems type V201, with a metallic stinger and the frequency response functions started to deviate over 700 Hz, well out of the region for this study. A Brüel&Kjær force sensor, of type 8203 with an IEPE converter 2647B, was used to measure the excitation force. Two small stinger attachment plates of 0.2 grammes each were glued at the two input positions. Direct transfer functions were obtained by placing accelerometers directly on the back side of the input position. This was considered best practice as the metal plates were flat and thin (approximately 2 mm). Three types of piezoelectric accelerometers were used, 10 triaxial PCB Piezotronic type 356A03 weighting 1 gramme each, 26 uniaxial PCB Piezotronic type PCB 352C22/NC weighting 0.5 grammes each and 1 uniaxial PCB Piezotronic type PCB 333B32 weighting 4 gramme. One triaxial accelerometer with its z component normal to the surface was used as direct acceleration at position 2 as seen in Figure 3a. Accelerometer 31 was of type PCB 333B32 and used as the direct acceleration for the second input, see Figure 3a. All accelerometers were attached with synthetic wax. It was difficult to orient the triaxial accelerometers with synthetic wax and keep the orientation during a vibration test, thus the x and y components must be considered more uncertain than the normal component.

Bolts were added to the structure, seen in Figure 2b, due to contact between two metal parts that caused non-linear effects. Two small wedges were also placed between two metal sheets due to possible contact between the two areas, and because it was found that the modes exciting this area, modes 4 to 7 seen in Figure 5e to 5h, greatly varied between the three components. To place accelerometers firmly on the exhaust hangers it was necessary to glue washers at the hangers. The same alterations were added to the FE model.

Multiple tests were performed for two types of excitation methods. For each input a periodic chirp, from 5 to 700 Hz, was performed at different amplitudes to rule out non-linearities. Then the calibration data was gathered from an adaptive multisine test where 10 frequencies were sent to the shaker simultaneously. The improved frequency selection [10] for system identification with N4SID [11] was used in a frequency range from 40 to 700 Hz with 8200 frequency lines for the multisine test.

A very good mathematical model must be identified from the measured data for good calibration results. Thus, the rigid body modes influence was subtracted from the experimental data by using the FE model rigid body modes. Three systems were then identified for the three components with the same model order, 38, that gave modes ranging from 50 to 490 Hz. Rigid body modes and a few residual high frequency modes with very low damping were manually added to the obtained systems and a reestimation of the state-space model's \mathbf{B} and \mathbf{C} matrices was performed with the multisine data used in the identification procedure. Data from the chirp testing in the region from 10 to 50 Hz was used in the reestimation, too. This resulted in a very good model that corresponded well to test data, even after damping equalisation. The equalisation was only performed on the

modes in the frequency range of interest, doing so on the manually added rendered a very poor estimate. Some channels gave poorer fit than others, and those were chosen as validation data, as the validation procedure uses raw data and no identified model is needed. Thus the validation channels selected from the 31 accelerometers or, 47 channels, for both inputs were $\{2, 5, 7, 9, 12, 13, 17, 18, 24, 27, 30, 32, 34, 36, 38, 40, 42, 43\}$. In Figure 3, with x , y , and z components for the triaxial sensors, this represents the following accelerometers $\{1_y, 2_y, 3_x, 3_z, 4_z, 5_x, 6_y, 6_z, 8_z, 11, 14, 16, 18, 20, 22, 24, 26, 27\}$.



(a) Front view of the subframe with input at location 31

(b) Closeup of subframe with input at location 2z

Figure 2 Front subframe shown in (a) with input at location 31, and (b) with input at location 2z

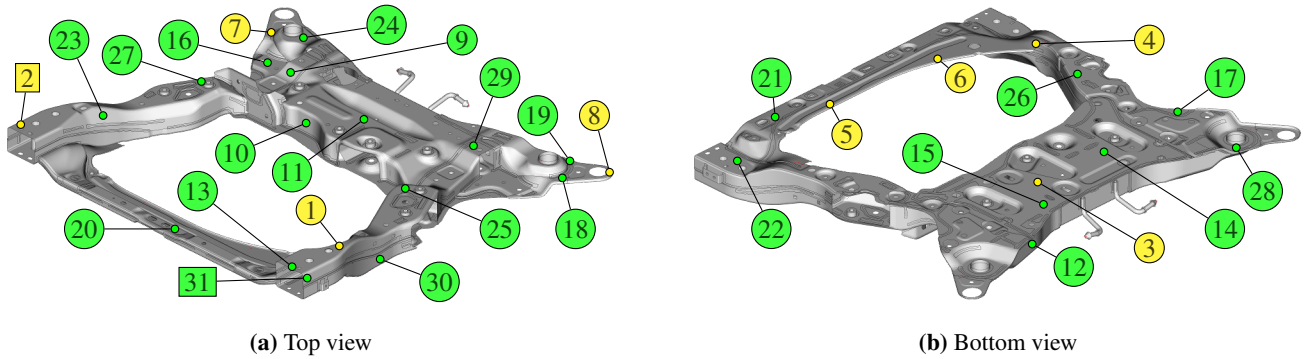


Figure 3 Top view of subframe in (a) and bottom view in (b) with colour markings. Yellow and green circles represent a triaxial and uniaxial sensor, respectively. The two square markings represent the input positions. The excitations were normal to the surface

3.2 Finite element model

The finite element model was updated to the best available CAD data. It was also verified visually that the FE model corresponded well to the three components. The thickness of the red highlighted part in Figure 4b was updated manually from direct measurement so that the FE model corresponded to the mean mass of the three component. The FE model consisted of 556,758 degrees-of-freedom with 96,550 shell elements, 11,017 solid elements, 6 CBAR elements, 23 groups of RBE2 elements and 22 groups of CONM2 elements. No verification of the mesh discretisation was performed as it was considered that the mesh quality was satisfactory.

The inverse Fisher information matrix (FIM) was used in an identifiability analysis to fix parameters that would render the calibration problem unidentifiable. Figure 4 indicates the different parameters, and their representation is shown in Table 1.

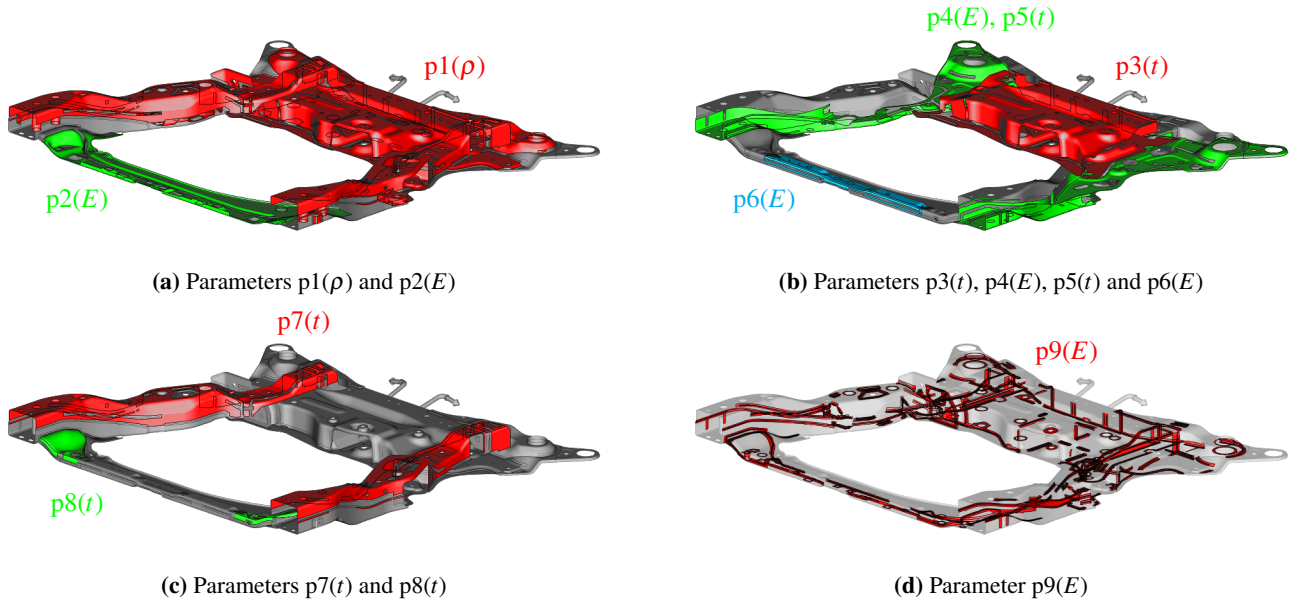


Figure 4 The 9 different parameters and their physical meaning, where ρ represent density, E stiffness and t thickness

Non highlighted parameters in Figure 4 were fixed to their nominal value. In short, three parameter types were used, stiffness, density and thickness. A lower and upper bound to these three types was decided to be approximately 20 %, with some deviations.

Four modes were found to be local around the exhaust hanger hooks, which can be seen at the top in Figure 2a. A sensitivity analysis was therefore performed to understand how sensitive they were to mass differences using a Rayleigh quotient analysis (RQ) [13].

$$RQ = \omega_n^2 = \frac{\phi_n^T \mathbf{K} \phi_n}{\phi_n^T \mathbf{M} \phi_n} = \frac{\omega_n^2}{1}, \quad \omega_n'^2 = \frac{\omega_n^2}{\phi_n^T (\mathbf{M} + \Delta \mathbf{M}) \phi_n} = \frac{\omega_n^2}{1 + \phi_n^T \Delta \mathbf{M} \phi_n} \quad (16)$$

Here ϕ_n is the eigenvector associated with the n :th eigenvalue ω_n^2 . A small mass perturbation $\Delta \mathbf{M}$ resulted in the new, approximate, eigenvalue $\omega_n'^2$. It was found that adding 4 grammes on the tip of each hanger made the first two local exhaust modes, mode 8 and 9 in the flexible mode order as seen in Figure 5i and 5j, switch place with flexible mode 7, seen in Figure 5h. The calibration was performed without considering these modes. A similar behaviour was found for three higher modes, 11, 12 and 13, seen in Figure 5l, 5m and 5n, respectively. One of these three higher modes was observable from test data and therefore used in the calibration.

4 Results from calibration, validation and bootstrapping

Three experimental datasets with 47 output channels and 2 input channels were used. The calibration set was formed with 29 output channels and 2 input channels and the validation set with 18 output channels and 2 input channels. Thus, approximately 38 % of the data was used for validation. The frequency region covered was from 55 to 430 Hz. The calibration was run with a damping equalisation of 0.2 %, 3 frequencies per half-band width, 100 Latin hypercube [14] samples, 20 start locations, including the nominal model, and maximum 100 iterations. While the calibration procedure uses data from the identified model, the calibration in the bootstrapping step is performed towards the raw data. Before the bootstrapping procedure the surrogate model is updated with respect to the improved parameter setting. In [12] it is proposed to run the bootstrapping $k = 100$ times. This was not feasible because of the large data sets used. Instead $k = 10$ was chosen. The surrogate model was created with model order 50 and 9 parameters. The nominal Young's modulus was 210 GPa and the density 7850 kg/m³. The thickness of the various parts varied from 4 mm to 1.6 mm. In Table 1 the parameters used in the calibration are described. It can be seen that there are some differences in the parameters between the three calibrated components. Most notably, all of them reach the lower bound set on parameter p6 and the upper bound on parameter p8. The bootstrapping results varies between the three calibrated components, but this was expected because real experimental data is used here. More interesting is that the coefficient of variation was 44 % for the thickness parameter p8 for component 3. This parameter had the largest variation for

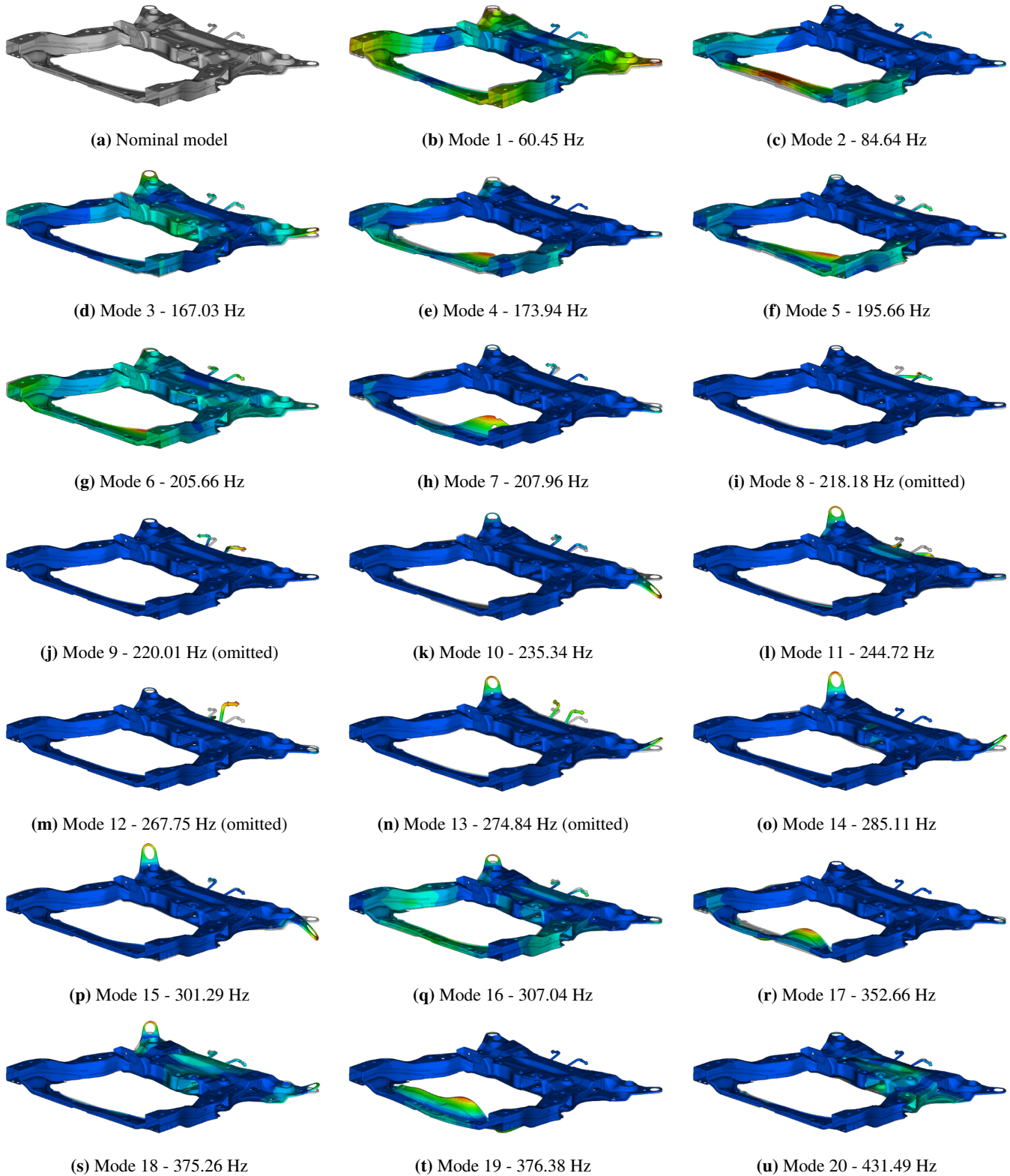


Figure 5 The nominal model (a) along with the 20 first non-calibrated modes, from mode 1 (b) to mode 20 (u). Blue indicate small modal motion and red large motion

Table 1 Nominal parameters, calibrated parameters denoted $FE_{c3\#}$, mean of bootstrapping parameters denoted FE_μ^B and their coefficient of variation (COV, %) denoted $FE_{COV\#}^B$ are shown. In this table E represent material stiffness, t denote thickness and ρ denote density

#	Parameter	Nominal	FE_{c1}	FE_{c2}	FE_{c3}	$FE_{\mu 1}^B$	$FE_{\mu 2}^B$	$FE_{\mu 3}^B$	FE_{COV1}^B	FE_{COV2}^B	FE_{COV3}^B
p1	$\rho [kg/m^3]$	7850.00	7299.31	7425.24	7411.31	7837.2	8531.21	7409.87	0.19	2.61	0.71
p2	$E [GPa]$	210.00	243.56	204.29	218.72	255.71	212.38	226.59	0.10	2.68	1.83
p3	$t [mm]$	2	1.82	1.79	1.79	1.88	1.98	1.73	0.07	2.23	3.33
p4	$E [GPa]$	210.00	234.44	234.94	226.99	231.07	254.25	214.83	0.36	2.22	2.06
p5	$t [mm]$	2	1.80	1.85	1.98	2.06	1.99	2.00	0.45	2.27	4.37
p6	$E [GPa]$	220.00	180.00	180.00	180.00	169.44	179.01	177.80	0.16	1.15	0.70
p7	$t [mm]$	2	1.88	1.84	1.86	2.25	2.34	1.83	0.41	5.54	3.97
p8	$t [mm]$	2	2.20	2.20	2.20	1.70	2.70	1.21	0.89	11.40	44.23
p9	$E [GPa]$	210.00	208.75	208.60	208.53	197.67	166.14	230.19	0.11	6.79	6.02

all three components. In Figure 4c it can be seen that this is a small part and it is connected to a region where many modes are locally active. It should be noted that the bootstrapping was run very few times and there was some deviation between the raw data and identified model which could partly explain the high spread in some of the parameters.

In Table 2 the eigenfrequencies for the three measured components are given, along with their mean μ and coefficient of variation COV in percent. Eigenfrequencies for the nominal FE model is also shown, followed by the eigenfrequencies for the three calibrations, one per component. The mean and coefficient of variation is also given for these three calibrations. Note that the 8th, 9th, 12th and 13th flexible modes from the FE model were omitted, as mentioned earlier. They were omitted by analysing their modeshapes and eigenfrequencies. It can be noted in Table 2 that the coefficient of variation between the three tested components is highest, 2.06 %, for mode 4 and lowest for mode 2 with a value of 0.15 %. It can also be noted that the modes that differ the most come in groups. This is most noticeable in modes 4 to 7. Mode 1, mode 13 and mode 15 also have a coefficient of variation larger than 1 %.

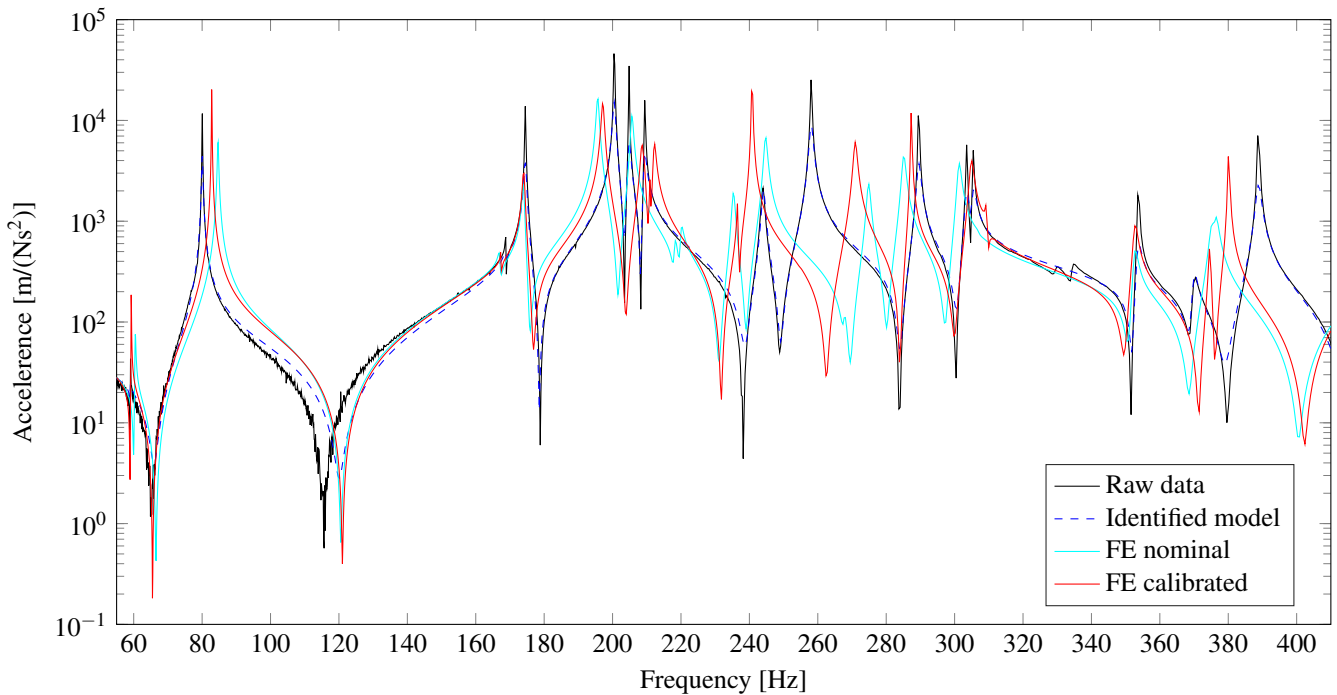
The deviation metric for calibration of component ID 1 is lowered by 21.60 % from 1.63 to 1.33 for raw measurement data. The validation metric decreases by 23.38 % from 1.76 to 1.35. For component ID 2 the calibration metric is reduced by 16.68 % from 1.59 to 1.28 and the validation metric is lowered by 17.59 % from 1.67 to 1.37. Lastly, for component ID 3 the calibration metric is reduced by 16.86 % from 1.56 to 1.31 and the validation metric is reduced by 16.28 % from 1.65 to 1.38. It is noticed that the calibration of component ID 1 was more successful than the two other, but also that the initial deviation was higher resulting in a similar calibration and deviation metric for the three components.

The FRFs of two different input output combinations are shown in Figure 6. It can be seen that the region between 310 and 350 Hz contains some spurious modes that were not identified and used in the calibration, but they were included in the bootstrapping. It can also bee seen that small improvements is gained from the calibration.

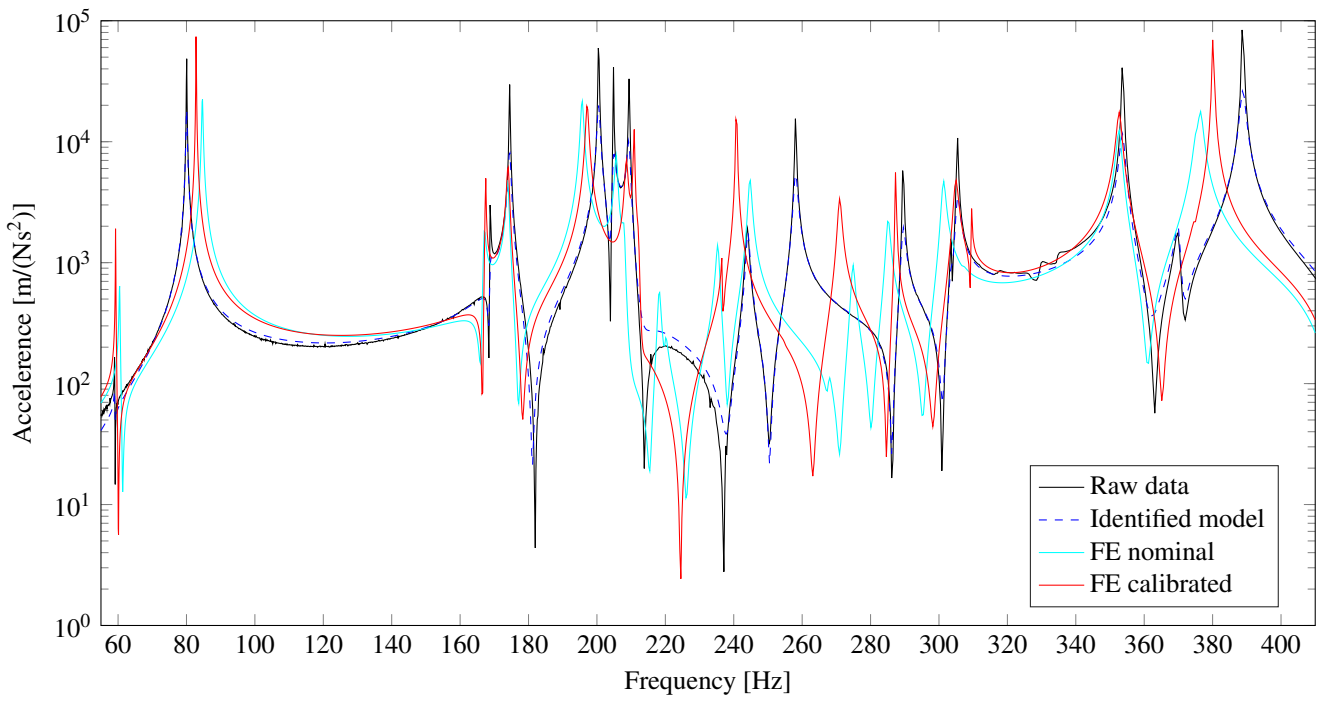
5 Conclusions

Three front subframe of a car have been calibrated, validated and uncertainties quantified with bootstrapping. The eigenfrequency variation between the thee components and the three calibrated FE models has been investigated, followed by the variations in the calibration parameters. It was found that the calibrated components had a similar deviation metric, from initially different metric values. Parameter p8 was found to be uncertain and parameters p6 and p8 were bound in the calibration procedure. Both of the parameters were located on the area where many modes were locally excited and it was believed, before calibration, that this area caused the difference between the components. The structure exhibited many local modes that were hard to measure accurately. A better parametrisation of the FE model is necessary for a better calibration outcome. Thus, further investigation is necessary in finding the reason for the deviation between the components and the FE model.

Considerable time was spent on performing the tests. The structures exhibited very different modal characteristics in some frequency intervals, while they were very equal in others. It was concluded that the plate seen in the middle bottom part of Figure 2a deviated in some way between the three components. It has also been concluded by investigating the FE model modeshapes in Figure 5 that many modes activated the outer thin rounded parts of the structure. There was no direct way of introducing a physical parameter to control these parts as they were connected to another part, together forming one large part of the structure, seen in green in Figure 4b. It is therefore believed that neither stiffness, density nor thickness are sufficient parameter types. Rather, a mapped thickness would probably yield better results. If no mapped thickness is available, a random



(a) Input at position 31 and output at 1x



(b) Input at position 31 and output at 5z

Figure 6 Frequency response functions of component ID 3 with raw data (black), identified model (dashed blue), nominal FE model (cyan) and calibrated FE model (red). In (a) the input is at position 31 while the output is at position 1x and in (b) the input is at position 31 and output is at position 5z (normal to the surface)

Table 2 Eigenfrequencies (Hz) for the 1st and up to the 15th flexible mode of the three components (ID #), the nominal FE model (FE_n) and the calibrated FE models ($FE_{c\#}$) against the three components are shown. Also, the mean (μ , Hz) and the coefficient of variation (COV, %) are given for each mode. For the FE model only the calibrated models are considered in the statistics

Mode	ID 1	ID 2	ID 3	ID $_{\mu}$	ID $_{COV}$	FE $_n$	FE $_{c1}$	FE $_{c2}$	FE $_{c3}$	FE $_{\mu}$	FE $_{COV}$
1	60.282	59.464	58.988	59.578	1.10	60.45	60.15	59.43	59.20	59.59	0.83
2	80.224	80.252	80.036	80.171	0.15	84.64	83.71	82.13	82.87	82.91	0.95
3	169.80	168.44	168.74	168.99	0.42	167.03	169.79	168.08	168.18	168.68	0.57
4	178.42	171.24	174.48	174.72	2.06	173.94	176.41	173.03	174.25	174.56	0.98
5	201.48	197.63	200.49	199.87	1.00	195.66	198.99	195.28	197.39	197.22	0.94
6	208.49	203.93	204.82	205.75	1.17	205.66	210.89	206.00	209.01	208.63	1.18
7	215.64	208.59	209.36	211.20	1.83	207.96	217.64	207.96	209.36	211.65	2.47
8	247.12	244.73	244.13	245.33	0.64	235.34	238.89	237.40	236.81	237.70	0.45
9	257.49	256.15	258.07	257.24	0.38	244.72	243.36	241.56	241.13	242.02	0.49
10	285.75	291.17	289.51	288.81	0.96	285.11	288.58	287.35	287.43	287.78	0.24
11	304.19	303.04	303.57	303.60	0.19	301.29	305.38	303.84	305.18	304.80	0.28
12	306.55	303.77	305.39	305.24	0.46	307.04	311.94	307.82	310.05	309.94	0.67
13	361.67	348.98	353.64	354.76	1.81	352.66	361.17	346.51	353.55	353.75	2.07
14	374.46	371.68	369.97	372.04	0.61	375.26	377.94	372.18	374.75	374.96	0.77
15	397.58	385.60	388.83	390.67	1.59	376.38	394.35	374.66	380.62	383.21	2.63

thickness variation in the part of interest would be another way to overcome the problem. Further, the curvature would be another interesting parameter to try out.

The calibration, validation and bootstrapping has been performed using the open source MATLAB program FEMcali, downloadable from Mathwork's webpage at www.mathworks.com.

Acknowledgement

Volvo Car Corporation is gratefully acknowledged for providing the funding for this paper.

References

1. Ewins, D. J. *Modal Testing: Theory, Practice and Application* 2nd Edition edition. 576 pp. (Wiley-Blackwell, Baldock, Hertfordshire, England; Philadelphia, PA, Sept. 20, 2000).
2. Friswell, M. I. & Mottershead, J. E. *Finite Element Model Updating in Structural Dynamics Solid Mechanics and its Applications* **38** (Springer Netherlands, 1995).
3. Abrahamsson, T. J. S. & Kammer, D. C. Finite element model calibration using frequency responses with damping equalization. *Mechanical Systems and Signal Processing* **6263**, 218–234 (Oct. 2015).
4. Abrahamsson, T. et al. Calibration and cross-validation of a car component using frequency response functions and a damping equalization technique in *26th International Conference on Noise and Vibration Engineering, ISMA 2014, Including the 5th International Conference on Uncertainty in Structural Dynamics, USD 2014* (2014), 2625–2640.
5. Abrahamsson, T. J. S. et al. Calibration and Validation of a Car Subframe Finite Element Model Using Frequency Responses in *Topics in Modal Analysis, Volume 10* (ed Mains, M.) 9–22 (Springer International Publishing, 2015).
6. Larsson, K.-J., Grétarsson, S. L., Vakilzadeh, M. K. & Abrahamsson, T. Calibration and Cross-Validation of a Car Component Model Using Repeated Testing in *Model Validation and Uncertainty Quantification, Volume 3* (eds Atamturktur, H. S., Moaveni, B., Papadimitriou, C. & Schoenherr, T.) 339–350 (Springer International Publishing, 2015).

7. Echaniz Granado, I. *Model calibration of a vehicle tailgate using frequency response functions*. Chalmers Student Theses. <<http://studentarbeten.chalmers.se>> (2015).
8. Kammer, D. C. Sensor set expansion for modal vibration testing. *Mechanical Systems and Signal Processing* **19**, 700–713 (July 2005).
9. Gibanica, M., Abrahamsson, T. J. S. & Kammer, D. C. Redundant information rejection in sensor localisation using system gramians in *Proceedings of the 34th IMAC* (Orlando, Florida, USA, Jan. 2016).
10. Khorsand Vakilzadeh, M., Yaghoubi, V., McKelvey, T., Abrahamsson, T. & Ljung, L. Experiment Design for Improved Frequency Domain Subspace System Identification of Continuous-Time Systems in *Proceedings of the 17th IFAC Symposium on System Identification* (Beijing, China, Oct. 20, 2015).
11. McKelvey, T., Akçay, H. & Ljung, L. Subspace-based identification of infinite-dimensional multivariable systems from frequency-response data. *Automatica* **32**, 885–902 (June 1996).
12. Hastie, T., Tibshirani, R. & Friedman, J. *The Elements of Statistical Learning - Data Mining, Inference, and Prediction* (Springer New York, 2009).
13. Craig, R. R. J. & Kurdila, A. J. *Fundamentals of Structural Dynamics* 2 edition. 744 pp. (Wiley, Hoboken, N.J, July 11, 2006).
14. McKay, M. D., Beckman, R. J. & Conover, W. J. Comparison of Three Methods for Selecting Values of Input Variables in the Analysis of Output from a Computer Code. *Technometrics* **21**, 239–245 (May 1, 1979).